metals

MDPI

Article

Low-Strain $KVPO_4F$@C as Hyperstable Anode for Potassium-Ion Batteries

Zhaomeng Liu [1,2,*], Da Wang [1], Yilong Zhang [1], Zhiqing Gong [1], Xuehui Lv [1], Qi Qin [1] and Yang Gong [1]

[1] Institute for Energy Electrochemistry and Urban Mines Metallurgy, School of Metallurgy, Northeastern University, Shenyang 110819, China
[2] Key Laboratory of Advanced Energy Materials Chemistry (Ministry of Education), Nankai University, Tianjin 300071, China
* Correspondence: liuzhaomeng@smm.neu.edu.cn; Tel.: +86-18940175152

Abstract: Potassium-ion batteries with carbon-based materials and alloy materials as anodes possess pronounced potassium storage and cycling abilities, yet they suffer from harsh synthetic processes, low initial Coulombic efficiency, and limited structure stability. Herein, we first put forward potassium vanadium fluorophosphate ($KVPO_4F$) as a highly stable anode material for potassium-ion batteries (PIBs). $KVPO_4F$@C composite is successfully synthesized through hydrothermal method followed by a low-temperature roasting process. An amorphous carbon film is homogeneously wrapped on the surface of the $KVPO_4F$ particles to improve electronic conductivity. As the anode for PIBs, the $KVPO_4F$@C presents a super-high discharge capacity of 242.32 mAh g^{-1} and a superior cycle stability over 120 cycles at 100 mA·g^{-1} with 93.1% capacity retention. Additionally, it maintains 92.9% of its initial capacity of 100 mA·g^{-1} at 1000 mA·g^{-1} after cycling 2100 times, which indicates an excellent long cycling performance. The in situ X-ray Diffraction and ex situ Transmission Electron Microscopy tests prove the minimal volume variation and stable structure of $KVPO_4F$@C. The designed $KVPO_4F$@C provides facilitative electronic conductivity and stable structure, successfully innovating an ultra-stable and high-performance anode material for potassium-ion batteries and other energy storage application fields.

Keywords: anode; potassium-ion batteries; $KVPO_4F$; long cycle; low-strain

check for updates

Citation: Liu, Z.; Wang, D.; Zhang, Y.; Gong, Z.; Lv, X.; Qin, Q.; Gong, Y. Low-Strain $KVPO_4F$@C as Hyperstable Anode for Potassium-Ion Batteries. *Metals* **2023**, *13*, 1038. https://doi.org/10.3390/met13061038

Academic Editor: Gabriele Mulas

Received: 15 March 2023
Revised: 3 May 2023
Accepted: 26 May 2023
Published: 29 May 2023

Copyright: © 2023 by the authors. Licensee MDPI, Basel, Switzerland. This article is an open access article distributed under the terms and conditions of the Creative Commons Attribution (CC BY) license (https://creativecommons.org/licenses/by/4.0/).

1. Introduction

The vigorous development of science and technology brought unprecedented brilliancy to human society. The continued consumption of fossil fuels makes the demand for clean, renewable, and sustainable energy sources ever-growing. Due to the intermittency, volatility, and uneven spatial distribution of renewable energy such as water energy, wind energy, and solar energy, as well as the irreversible trend of vehicle electrification and the rapid increase of the energy storage market, electrochemical energy storage systems have ushered in significant development opportunities. Among the various electrical energy systems, secondary batteries are extensively investigated because they are environmentally friendly, convenient, recyclable, and have high safety [1–5]. Thereinto, as one of the most promising secondary battery systems, lithium-ion batteries (LIBs) own several advantages such as high energy density and power density, low self-discharge rate, and small size [6–8]. However, the battery manufacturing costs increase continually because the scarcity and excessive consumption of lithium resources [9–11]. It is necessary to design a new battery system with low cost, energy density, power density, and cycle stability comparable to lithium-ion batteries to make up for the shortage of lithium-ion batteries.

The reserves of sodium and potassium elements, both of which are alkali metals, are almost 1000 times that of lithium reserves in the Earth's crust. Their prices are much lower than lithium and their properties are similar to lithium. Therefore, the material system and industrialization process of lithium-ion batteries can be learned and the application can be

carried out in other alkali metal battery systems. Sodium-ion batteries have been widely examined and some research progress has been made. Potassium-ion batteries have as great research value and application potential as sodium-ion batteries. They work in a similar way to lithium-ion batteries by shuttling potassium ions between positive and negative electrodes. Meanwhile, compared with the standard hydrogen electrode potential, the redox potential of lithium, sodium, and potassium is −3.04 V, −2.71 V, and −2.93 V, respectively. Potassium is more negative than sodium and more similar to lithium. Potassium-ion batteries may provide a higher voltage than sodium-ion batteries, depending on if the voltage provided by the battery is equal to the potential difference between the positive and negative electrodes when other parameters are kept similar. Owing to natural abundance and low cost of potassium resources, potassium-ion batteries (PIBs) have recently captured growing interest as one of the most beneficial electric energy storage systems [12–14]. The really low redox potential (−2.94 V) of the K^+/K couple contributes to the high work potential and energy density, which reveals a superior application prospect of PIBs for sustainable energy storage technology [15–18]. However, as one of the key components, the mainstream negative electrodes for PIBs suffer from serious problems, in terms of the pulverization phenomenon of graphite, the serious volume expansion of the metals and metal oxides/sulfides/phosphates, and low initial Coulombic efficiency of hard/soft carbon [19–22]. Therefore, it is of great significance to put forward an innovative electrode to meet the development needs of potassium-ion batteries.

In view of the low raw material price and high security, triclinic $LiVPO_4F$ and $NaVPO_4F$, the framework materials based on phosphate polyanion, have been widely investigated as cathode materials because of their high operating voltage and excellent thermal stability [23–26]. Interestingly, there is a special insertion reaction at around 1.8 V associated with the V^{2+}/V^{3+} redox couple, indicating the potential of lithium or sodium vanadium fluorophosphate as an anode material [7,19,27]. There are many studies describing the existence and the key role of fluorine in the work of $KVPO_4F$ materials and focus on the improvement of electrochemical performance [27–29]. The synthesis method of $KVPO_4F$ materials mainly includes carbothermal reduction method, sol-gel method, hydrothermal method, ion exchange method, and so on [28–31]. The research ideas of material modification that can be used for reference mainly focus on the substitution of beneficial elements, conductive substances, and coating modification of fast ion conductors [32–35]. Hence, we can speculate that potassium vanadium fluorophosphate ($KVPO_4F$) possesses a bright possibility to be a potential anode material for potassium-ion batteries [28–31]. However, there are few papers putting forward the key effect about potassium ions storage of $KVPO_4F$ at low operating voltages [32–35]. In addition, owing to the low electronic conductivity (i.e., 1.84×10^{-5} $S \cdot m^{-1}$) and the unstable electrode/electrolyte interface, $KVPO_4F$ as an electrode material suffers an inferior cycling and rate performance [36–39]. According to the modification examples of polyanionic materials in lithium-ion batteries and sodium-ion batteries fields, in situ substitution of elements can change the internal structure of materials, improve the ion transport of materials, and make the material structure more stable by using lattice defects such as negative/cation vacancy [39]. The coating of conductive carbon material and fast ion conductor can increase the interface stability between the electrode particle interface and electrolyte, which is a very effective modification method [40]. Therefore, $KVPO_4F$ as anode for PIBs with superior electrochemical performance is urgently needed to be explored.

Herein, we design the $KVPO_4F$@C composite via hydrothermal method assisted by a facile sintering process for the first time [20,40,41]. In this composite, the homogeneous carbon layer coating on the surface of the $KVPO_4F$ particle is formed in situ as a conductive network for improved electronic conductivity. The $KVPO_4F$ primary particles uniquely stack to form micron-sized secondary particles during hydrothermal process. The $KVPO_4F$@C as anode material is fully investigated. Due to the superior electronic conductivity and structural flexibility, $KVPO_4F$@C as anode shows a discharge capacity of 242.32 $mAh \cdot g^{-1}$ and a superior cycle stability over 120 cycles at 100 $mA \cdot g^{-1}$ with a

93.1% capacity retention. In addition, after cycling 2100 times at 1000 $mA \cdot g^{-1}$, $KVPO_4F$@C reveals the specific charge capacity of 100 $mA \cdot g^{-1}$ and maintains a 92.9% capacity retention, which indicates an excellent long-life cycling performance. Thus, a $KVPO_4F$@C composite is a highly ideal anode material for developing the ultra-stable potassium-ion batteries.

2. Materials and Methods

Synthesis: The $KVPO_4F$@C composite was synthesized via a simple hydrothermal reaction route assisted by a low-temperature pre-roasting and sintering process. These are the detailed steps: firstly, potassium fluoride KF (Metal level), vanadium pentoxide V_2O_5 (A.R., 99%), diammonium hydrogen phosphate $NH_4H_2PO_4$ (A.R., 99%), and oxalic acid dihydrate $H_2C_2O_4 \cdot 2H_2O$ (A.R., 99.5%) (with 20% excess of the stoichiometric amounts) were dissolved in deionized water to obtain an orange-yellow solution. $H_2C_2O_4 \cdot 2H_2O$ acted as the reductant and carbon source. Then, the solution was transferred to a 200 mL Teflon-lined autoclave and kept at 200 °C for 24 h. After naturally cooling down, the black precipitate was filtered and washed separately with distilled water and ethanol three times, followed by drying under vacuum oven at 60 °C for 12 h. The obtained powder was applied as precursor. Finally, the as-prepared precursor was annealed at 350 °C for 2 h for pre-roasting, and then roasted at 680 °C for 6 h in a tube furnace, the roasting process is under argon atmosphere. Both heating and cooling rates are 2 $°C \cdot min^{-1}$. The as-obtained black sample was named as $KVPO_4F$@C.

Material characterizations: The micro-morphologies of $KVPO_4F$@C were conducted by the Field Emission Scanning Electron Microscope (FESEM, Hitachi S-4800, 20 kV). The microstructure of the synthesized $KVPO_4F$@C was conducted by the Transmission Electron Microscopy (TEM, Titan G2 60-300). The Powder X-ray Diffraction (XRD, Rint-2000, Rigaku, Cu Kα) was employed to confirm the crystal structures of $KVPO_4F$@C. The Energy Dispersive Spectrometer (EDS) mapping analysis was employed to confirm the elemental distributions of $KVPO_4F$@C. Carbon–sulfur analyzer equipment (Eltar, Germany) was employed to confirm the carbon content in the samples. The in situ XRD (Bruker AXS, D-76187, Karlsruhe, Germany) and ex situ TEM and XPS (XPS, Thermo Scientific K-Alpha) were carried out to investigate the structure and morphology changes of $KVPO_4F$@C anode during cycling. The electrodes, obtained by disassembling the half-cells in the glove box, need to be washed with the DME (Dimethoxyethane) solution several times and dried in vacuum prior to the observations. The inductively coupled plasma atomic emission spectrometry (ICPAES, IRIS intrepid XSP, Thermo Electron Corporation) was employed to ascertain the loss mass content of elemental V dissolved in cycled cells.

Electrochemical tests: The electrochemical tests with $KVPO_4F$@C as anode for PIBs were conducted by assembling the CR2032 coin-type cells. The detailed steps of the working electrode fabrication were as follows: $KVPO_4F$@C (active material), polyvinylidene fluoride (binder), and acetylene black (conductive agent) with a ratio of 8:1:1 were fully mixed and ground for 0.5 h, then, the mixture was decanted into a small bottle with appropriate N-methyl pyrrolidinone (NMP) solution and stirred for 12 h to form slurry. The slurry was spread on the smooth copper foil (current collector), and then dried at 120 °C for 6 h in a vacuum oven. It was punched into rounded pieces and the working electrodes were acquired with an area of 1.13 cm^2. The average weight of the active material on each piece weighs about 1.6~2.0 mg. We assembled the Coin-type cells in a dry Ar-filled glove box. The counter electrode was rounded potassium metal pieces, and the cellulose paper was employed as the separator. The electrolyte was 3 M KFSI (Potassium difluorosulfonimide) in DME (Dimethoxyethane) solvent. The electrochemical tests were conducted via an automatic galvanostatic battery testing system by NEWARE, as the battery circler has a potential range of 0.01–3.0 V. Cyclic voltammetry (CV) of $KVPO_4F$@C as anode was tested with the CHI660A electrochemical analyzer. We carried out the CV tests within the voltage range from 0.01 to 3.0 V at the scanning rate of 0.1 mV $s^{-1} \cdot h$.

In order to investigate the structural stability mechanism and the loss of vanadium from $KVPO_4F$@C during electrochemical process, we disassembled the cells with $KVPO_4F$@C

as anode after cycling at 3.0 V after the first time and 100 times. The pole pieces were immersed in DME solution several times in 0.5 h for further investigation of the morphology and property changes. In order to investigate the lost vanadium, the cycled cells were disassembled and dissolved in the washing solution. Then, the washing liquid was selected and dissolved in hydrochloric acid, and the content of vanadium was determined by ICP equipment. By comparison, we can confirm the loss rate of vanadium in electrolyte.

3. Results and Discussion

Figure 1a depicts a schematic illustration of synthetic steps for the synthesis of the designed $KVPO_4F$@C composite. The prepared raw materials were mixed in deionized water with continuous stirring; then the mixed raw material agglomerated into a micro-sized spherical precursor after hydrothermal reaction. The obtained precursor shows hexagonal shape; it transformed into secondary particles through the low-temperature roasting process. Figure 1b shows the XRD pattern of the $KVPO_4F$@C composite; the high-intensity characteristic peaks of $KVPO_4F$ were detected, indicating that the synthesis method has successfully produced the crystalline $KVPO_4F$, which exhibits the high-intensity characteristic peaks of $KVPO_4F$ without any peaks from impurities found, indicating that the crystalline $KVPO_4F$ with a high purity was successfully produced by the simple synthesis method. In addition, at around 26.5°, there is no distinctive peak associated with pyrolytic carbon found. It can be put down that the carbon phase in the composite is in an amorphous state. The carbon content in $KVPO_4F$@C is about 1.1 wt.% from the carbon–sulfur (C–S) analysis. This is a very small mass ratio of carbon element in composite, which places less interference on the capacity of $KVPO_4F$@C. In addition, the existence of pyrolytic carbon can hinder the fluorine loss during the roasting action, which effectively avoids the impurities under the high temperatrue treatment. The $KVPO_4F$@C composite has better electronic conductivity because of the amorphous carbon layer coating on the surface of particles. Figures 1c,d and S1 show the SEM images of $KVPO_4F$@C particles, it is obvious that the micron-sized secondary particles and hexagonal primary particles are formed by the hydrothermal reaction, and the particles in the size distribution are micro-size since the large particles are aggregated from the smaller nano-size ones.

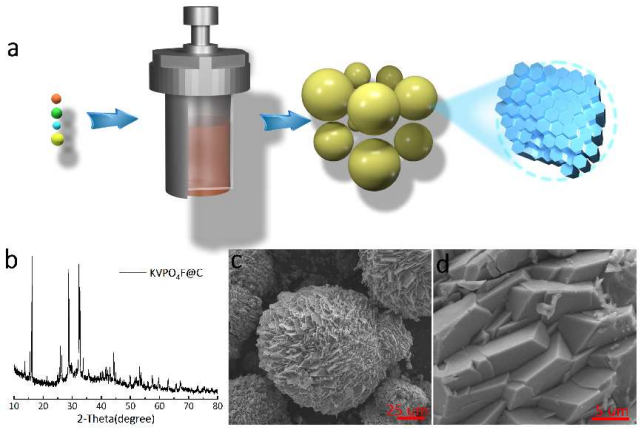


Figure 1. (**a**) Schematic illustration for the synthesis of $KVPO_4F$@C composite material. (**b**) XRD curve of the $KVPO_4F$@C sample. (**c**,**d**) SEM images of prepared $KVPO_4F$@C particles with different enlargement factors showing the stacked hexagonal structure.

In order to further study the micro-morphologies of $KVPO_4F$@C, TEM, HRTEM, and EDS mappings tests were carried out. As shown in Figures 2a and S2, the TEM image of $KVPO_4F$@C shows the regular outline and the reunion action from primary particles to secondary ones. In addition, potassium vanadium fluoride phosphate material has a large size distribution at micron scale, and the internal structure of the synthesized material is compact, which indicates the high compaction density of $KVPO_4F$@C. There is residual

carbon on the surface of the $KVPO_4F$ particles, which is left after the reduction reaction during the roasting process. The existence of pyrolytic carbon can effectively increase the electronic conductivity of synthetic $KVPO_4F$@C composite material, which makes it a beneficial material to apply as the electrode for battery systems. Figure 2b exhibits the enlargement of a single $KVPO_4F$@C particle, which illustrates a hexagonal micro-sized structure. The hexagonal structure is formed by the hydrothermal reaction. The shape of the particle is similar to a brick, which is conducive to scattered stacking, forming a stable architecture. From the HRTEM image (Figure 2c), it is obvious that the $KVPO_4F$ crystals are identified, whose surfaces are wrapped by the amorphous carbon layer. The designed core/shell structure of $KVPO_4F$@C can give rise to a stable electrode surface. The stable electrode surface hinders the corrosion reaction at the electrode/electrolyte surface, constructing a comfortable charge and discharge cycling environment. EDS mappings of $KVPO_4F$@C are presented in Figure 2d; it is obvious that K, F, P, V, and O elements distribute a similar outline to the bulk nanoparticle, indicating the $KVPO_4F$ core. In addition, there is C element found partly surrounding the inner particle. Such a large hexagonal structure can effectively boost the tap density. From the EDS and TEM results, it is obvious that amorphous pyrolytic carbon is wrapped on the surfaces of $KVPO_4F$@C particles, which can effectively connect multiple $KVPO_4F$@C particles. The amorphous carbon coating layer is formed by stacking flexible carbon film nanosheets during the roasting progress. In a nutshell, this special route achieved the fabrication of $KVPO_4F$@C composite through roasting precursor from the hydrothermal process to build a special structure.

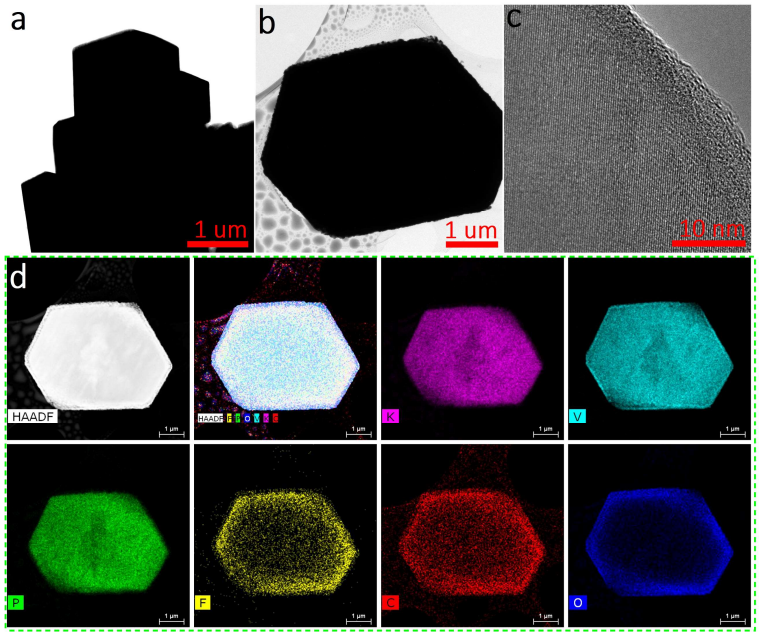


Figure 2. Morphology of the $KVPO_4F$@C composite material. (**a**) The microstructure of $KVPO_4F$@C secondary particle conducting by TEM; (**b**) TEM image of the single $KVPO_4F$@C particle; (**c**) HRTEM image revealing the interface of $KVPO_4F$ and carbon phase; (**d**) EDS mappings result presenting the distribution of K, V, P, F, C, and O elements in the $KVPO_4F$@C composite.

Cycle performances of $KVPO_4F$@C as anode material for potassium-ion batteries are fully tested. The initial three consecutive cyclic voltammetry (CV) curves at 0.1 $mV \cdot s^{-1}$ are depicted in Figure 3a. There are two broad characteristic peaks located at around 1.03 V and 0.81 V in the initial cycle ascribed to the formation of solid electrolyte interface (SEI), which builds a stable interface between electrode and electrolyte. Two pairs of reduction/oxidation peaks are located at around 0.81/1.0 V and 1.02/1.26 V during the first whole (de)intercalation process, which associates with the insertion/extraction of K^+ ions into/out of the crystal lattice of $KVPO_4F$@C anode. The CV curves in the next two

cycles display the similar two pairs of reduction and oxidation peaks, which are located at 1.00 V and 1.26 V, respectively. The same outline of CV curves is because of the stable solid electrolyte interface (SEI) formed during the first cycling process. The constant polarization represents $KVPO_4F$@C anode possessing a stable cyclic environment after first cycling. Figure 3b shows the initial charge/discharge profiles of $KVPO_4F$@C at 100 mA·g^{-1}, which possess the reversible specific charge capacity of 242.32 mAh·g^{-1} corresponding to the initial Coulombic efficiency of 50.6%. This working plateau is higher than the plateau of traditional graphite, which can avoid the dendritic effect of potassium metal. The cycling performances of $KVPO_4F$@C are displayed in Figure S3. The $KVPO_4F$@C anode achieves an initial specific charge capacity of 242.32 mAh·g^{-1} at 100 mA·g^{-1}, and it still maintains a capacity as high as 225.59 mAh·g^{-1} even after being cycled 120 times, equivalent to a high-capacity retention of 93.1%. The rate performance of $KVPO_4F$@C at various current densities is shown in Figure 3c. It is worth noting that the designed $KVPO_4F$@C exhibits much higher capacity at high current densities of 4000 mA·g^{-1}. Specifically, the $KVPO_4F$@C anode reveals the superior reversible capacities about 242.32, 195.23, 175.60, 160.78, 104.34, and 92.42 mAh·g^{-1} when charged at the increasing current densities of 100, 200, 500, 1000, 2000 and 4000 mA·g^{-1} 20 times, respectively. In addition, the charge capacity could recover to its original value when the current density returns to 100 mA·g^{-1}, which indicates a superior recoverability rate of $KVPO_4F$@C. The charge–discharge curves of $KVPO_4F$@C at different current densities are shown in Figure S4. The long-term cycling performance of this special $KVPO_4F$@C is revealed. As displayed in Figures 3d and S5, the $KVPO_4F$@C exhibits an excellent cycling performance, achieving a specific charge capacity of 160.24 mAh·g^{-1} with a capacity retention of about 92.9% after cycling 2100 times at the high current density of 1 A·g^{-1}. The super specific capacity, excellent rate property, and outstanding long-term cycling performance together with high-capacity retention demonstrate that the designed $KVPO_4F$@C is an ideal choice as the anode material for potassium-ion batteries.

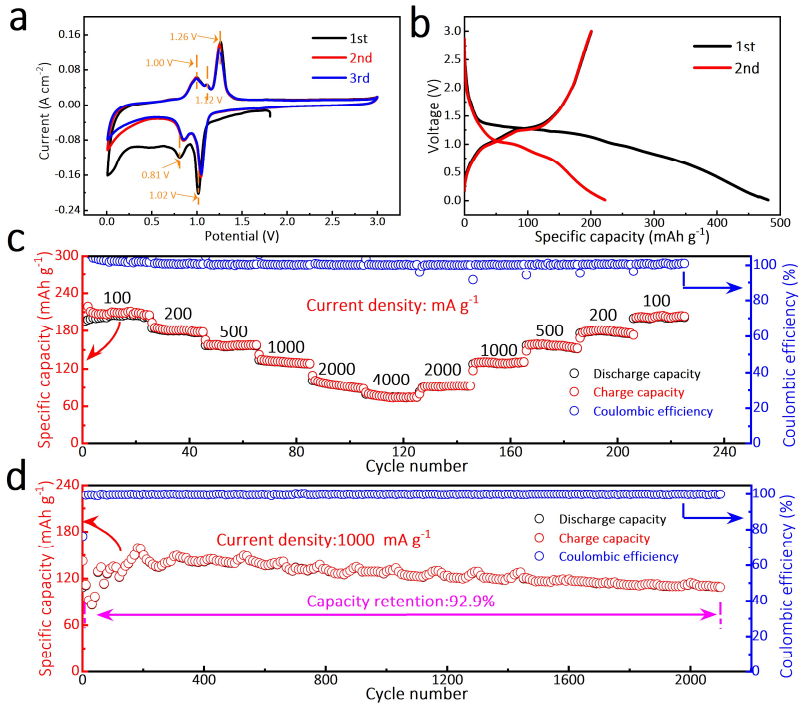


Figure 3. Electrochemical performance of as–prepared $KVPO_4F$@C composite as anode for PIBs. (**a**) CV curves at 0.1 mV s^{-1} with the potential window ranging from 0.01 V to 3.0 V; (**b**) The initial and the second cycling curves in the potential range from 0.01 to 3.0 V at the current of 300 mA·g^{-1}; (**c**) Rate capability of $KVPO_4F$@C in the rate ranging from 100 to 4000 mA·g^{-1}; (**d**) Cycling stability of $KVPO_4F$@C as anode for PIBs at the current density of 1000 mA·g^{-1} cycling 2100 times.

It is well known that potassium-ion battery anode materials suffer poor cycling performance below room temperature. Anode materials for potassium-ion batteries react with organic solvents in the electrolyte, especially at low temperatures, resulting in rapid capacity decay. Therefore, it is urgent to improve the electrochemical performance at low temperatures in practical applications. To evaluate the electrochemical performance of $KVPO_4F$@C at lower than room temperature, charge–discharge tests under 20 °C were conducted at 100 $mAh{\cdot}g^{-1}$ 100 times. In Figure S6a, the initial discharge specific capacity of $KVPO_4F$@C (227.2 $mAh{\cdot}g^{-1}$) at 20 °C is similar to that of $KVPO_4F$@C at 25 °C (225.6 $mAh{\cdot}g^{-1}$), and both show similar charge capacities (247.2 $mAh{\cdot}g^{-1}$ at 20 °C and 242.3 $mAh{\cdot}g^{-1}$ at 25 °C). As a result, $KVPO_4F$@C reveals 91.9% initial Coulombic efficiency at 20 °C, close to that of $KVPO_4F$@C at 25 °C (93.1%). In addition, with the pyrolytic carbon coating, the cycle performance at low temperature remains stable. As shown in Figure S6b, $KVPO_4F$@C maintains a discharge capacity of 213.6 $mAh{\cdot}g^{-1}$ with 94.1% capacity retention after cycling 100 times, indicating the superior comprehensive electrochemical performance of $KVPO_4F$@C.

To investigate in-depth knowledge about K ions storage mechanism of $KVPO_4F$@C as anode, the morphologies transformation and structural evolution of the tested electrodes after specific cycling were significantly explored. As exhibited in Figure 4a,b, the cycling curves at 100 $mA{\cdot}g^{-1}$ and the corresponding in situ XRD analysis were tested to achieve the structural evolution of $KVPO_4F$@C in the initial two cycles. It is obvious the $KVPO_4F$@C crystalline structure has changed during the K^+ ions insertion/extraction process. During the charging process, the dominant peak located at 32.49° of $KVPO_4F$@C disappeared, and it reappeared after a whole cycling process. During the deeply embedded K^+ ion process, there exists a very significant peak migration as a fresh phase appears at about 31.46°, which is associated with the V^{2+}/V^{3+} redox couple. The results reveal that the K^+ ions reversibly diffuse into/out of the $KVPO_4F$ crystal lattice with admirable structural stability. As well, the characteristic peak migrates from 31.46° back to 32.49° during the K^+ extraction process. Therefore, although the K ions insertion reaction is accompanied by a little volume expansion, $KVPO_4F$@C still keeps the superior reversibility. This phenomenon indicates that during the incorporation of K^+ into the $KVPO_4F$ crystal lattice, there is a low degree of structural arrangement. The TEM and HRTEM images of $KVPO_4F$@C anode discharged to 0.01 V after 100 cycles are shown in Figures 4c–e and S7. The complete micro-sized particles possessing a regular hexagonal structure are observed (Figure 4c,d), which has the same diameter compared with the pristine $KVPO_4F$@C, indicating that $KVPO_4F$@C electrode shows no obvious volume expansion during the K^+ ions insertion process. The HRTEM image in Figures 4e and S8 further verifies the relationship between the evolution of $KVPO_4F$ microstructure and potassium-ions storage. The HRTEM image in Figure S8 shows a complete and clear $KVPO_4F$ lattice with nano-sized carbon thin film coating on the surface of the particle. It is obvious that the overall structure of $KVPO_4F$@C can be well maintained after 100 times of the fully discharge cycling process, further demonstrating excellent structural stability. According to the test data, the loss of vanadium element in $KVPO_4F$@C electrode is about 0.18 wt% after cycling 100 times. The pyrolytic carbon coating layer acts as a physical protection barrier to suppress harmful side reactions and enhance the chemical stability of $KVPO_4F$ cores in $KVPO_4F$@C, resulting in a stable cycle performance.

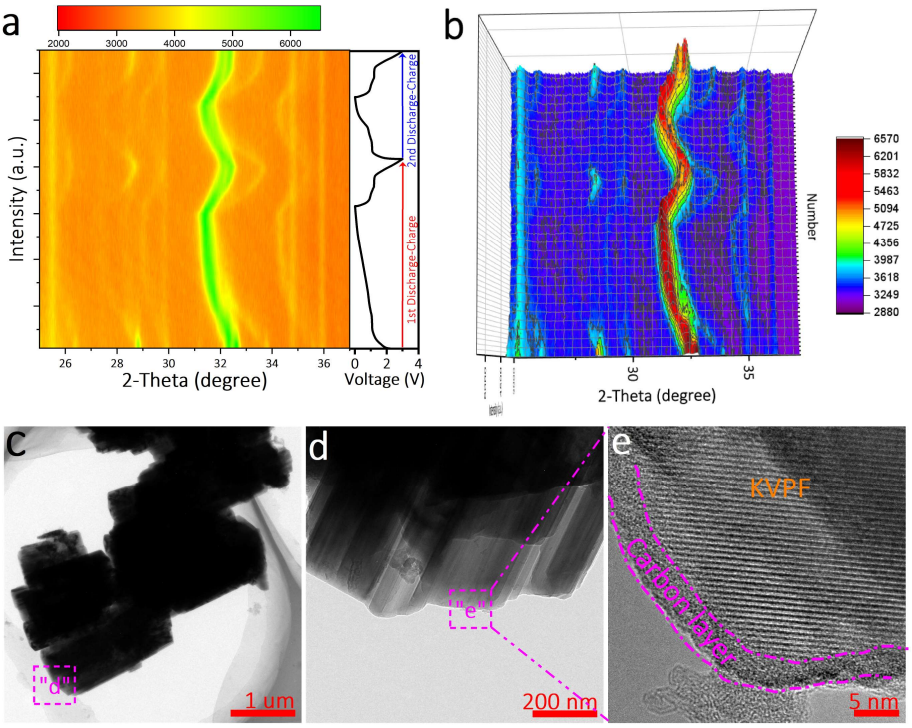


Figure 4. Structure and morphology of $KVPO_4F$@C as anode for PIBs after the specified cycling time. (**a**) Selected cycling curves of $KVPO_4F$@C as anode for PIBs at the initial two cycles. (**b**) The related in situ XRD patterns of $KVPO_4F$@C during the initial two cycles. (**c**–**e**) Typical TEM, enlarged TEM, and HRTEM images of $KVPO_4F$@C cycling after 100 cycles at 100 $mA{\cdot}g^{-1}$ prove the excellent structural stability.

4. Conclusions

In summary, the designed $KVPO_4F$@C composite was successfully synthesized via a simple hydrothermal reaction process followed by a one-step low-temperature annealing process. In this composite, the huge $KVPO_4F$ particles were wrapped by the nano-sized amorphous carbon layer. $KVPO_4F$@C as anode for PIBs provides superior electrochemical performance, including an excellent rate property, a high K^+ ions storage voltage, and an ultra-stable long-cycle performance. Concretely, it delivers a reversible specific capacity of 242.32 $mAh{\cdot}g^{-1}$ with the initial Coulombic efficiency of about 50.6% and maintains a high capacity retention of about 93.1% at 100 $mA{\cdot}g^{-1}$ after cycling 100 times. In addition, ultralong cycle life at 1000 $mA{\cdot}g^{-1}$ is excavated, which possesses a high charge capacity of 160.24 $mAh{\cdot}g^{-1}$ with ~92.9% retained capacity after 2100 cycles. This work demonstrates a great impetus of utilizing $KVPO_4F$@C composite as an admirable anode for potassium-ion batteries and innovates a route for designing high-performance electrodes for other energy storage and conversion systems.

Supplementary Materials: The following supporting information can be downloaded at: https://www.mdpi.com/article/10.3390/met13061038/s1, Figure S1: (a) and (b) the SEM images of $KVPO_4F$@C showing the reunion behavior of primary particles; Figure S2: TEM images of bare $KVPO_4F$@C sample; Figure S3: Cycle performance of bare $KVPO_4F$@C at 100 $mA{\cdot}g^{-1}$ for 120 times; Figure S4: Selected charge/discharge curves at the current densities of 100, 200, 500, 1000, 2000 and 4000 $mA{\cdot}g^{-1}$; Figure S5: Selected 400th, 800th, 1200th, 1600th, and 2100th charge/discharge curves at the current density of 1000 $mA{\cdot}g^{-1}$; Figure S6: (a) Selected charge/discharge curves at the current densities of 100 $mA{\cdot}g^{-1}$ and (b) the cycle performance of $KVPO_4F$@C at 100 $mA{\cdot}g^{-1}$ for 110 times; Figure S7: TEM images of $KVPO_4F$@C anode after cycling for 100 times; Figure S8: HRTEM images of $KVPO_4F$@C anode after cycling for 100 times.

Author Contributions: Conceptualization, Z.L. and D.W.; methodology, Z.L.; software, D.W.; validation, Z.L., Y.Z. and Y.G.; formal analysis, Z.G.; resources, Z.L.; data curation, X.L. and Z.L.; writing—original draft preparation, Z.L. and Q.Q.; investigation, Z.L. and Q.Q.; writing—review and editing, Z.L.; visualization, Y.Z.; supervision, Z.L.; project administration, Z.L.; funding acquisition, Z.L. All authors have read and agreed to the published version of the manuscript.

Funding: This research was funded by the National Natural Science Foundation of China (Nos. 52204308), the Postdoctoral Science Foundation of China (No. ZX20220158), and the Postdoctoral Foundation of Northeastern University.

Conflicts of Interest: The authors declare no conflict of interest.

References

1. Cao, K.; Zhao, X.; Chen, J.; Xu, B.B.; Shahzad, M.W.; Sun, W.; Pan, H.; Yan, M.; Jiang, Y. Hybrid Design of Bulk-Na Metal Anode to Minimize Cycle-Induced Interface Deterioration of Solid Na Metal Battery. *Adv. Energy Mater.* **2021**, *12*, 2102579. [CrossRef]
2. Liao, J.; Chen, C.; Hu, Q.; Du, Y.; He, Y.; Xu, Y.; Zhang, Z.; Zhou, X. A Low-Strain Phosphate Cathode for High-Rate and Ultralong Cycle-Life Potassium-Ion Batteries. *Angew. Chem. Int. Ed. Engl.* **2021**, *60*, 25575–25582. [CrossRef] [PubMed]
3. Liao, J.; Han, Y.; Zhang, Z.; Xu, J.; Li, J.; Zhou, X. Recent Progress and Prospects of Layered Cathode Materials for Potassium-ion Batteries. *Energy Environ. Mater.* **2021**, *4*, 178–200. [CrossRef]
4. Shi, Q.; Qi, R.; Feng, X.; Wang, J.; Li, Y.; Yao, Z.; Wang, X.; Li, Q.; Lu, X.; Zhang, J.; et al. Niobium-Doped Layered Cathode Material for High-Power and Low-Temperature Sodium-Ion Batteries. *Nat. Commun.* **2022**, *13*, 3205. [CrossRef] [PubMed]
5. Tsuchimoto, A.; Shi, X.M.; Kawai, K.; Mortemard de Boisse, B.; Kikkawa, J.; Asakura, D.; Okubo, M.; Yamada, A. Nonpolarizing Oxygen-Redox Capacity without O-O Dimerization in $Na_2Mn_3O_7$. *Nat. Commun.* **2021**, *12*, 631. [CrossRef]
6. Liu, S.; Shao, W.; Zhang, W.; Zhang, T.; Song, C.; Yao, M.; Huang, H.; Jian, X.; Hu, F. Regulating Microstructures of Soft Carbon Anodes by Terminations of Ti_3C_2T MXene toward Fast and Stable Sodium Storage. *Nano Energy* **2021**, *87*, 106097. [CrossRef]
7. Liu, Z.; Peng, W.; Shih, K.; Wang, J.; Wang, Z.; Guo, H.; Yan, G.; Li, X.; Song, L. A MoS_2 Coating Strategy to Improve the Comprehensive Electrochemical Performance of $LiVPO_4F$. *J. Power Sources* **2016**, *315*, 294–301. [CrossRef]
8. Wu, Y.; Cao, Z.; Song, L.; Gao, J. $NaFe_2PO_4(MoO_4)_2$: A Promising NASICON-Type Electrode Material for Sodium-Ion Batteries. *ACS Appl. Mater. Interfaces* **2021**, *13*, 48865–48871. [CrossRef]
9. Kim, H.; Seo, D.-H.; Urban, A.; Lee, J.; Kwon, D.-H.; Bo, S.-H.; Shi, T.; Papp, J.K.; McCloskey, B.D.; Ceder, G. Stoichiometric Layered Potassium Transition Metal Oxide for Rechargeable Potassium Batteries. *Chem. Mater.* **2018**, *30*, 6532–6539. [CrossRef]
10. Nathan, M.G.T.; Yu, H.; Kim, G.T.; Kim, J.H.; Cho, J.S.; Kim, J.; Kim, J.K. Recent Advances in Layered Metal-Oxide Cathodes for Application in Potassium-Ion Batteries. *Adv. Sci.* **2022**, *9*, e2105882. [CrossRef]
11. Yao, L.; Zou, P.; Wang, C.; Jiang, J.; Ma, L.; Tan, S.; Beyer, K.A.; Xu, F.; Hu, E.; Xin, H.L. High-Entropy and Superstructure-Stabilized Layered Oxide Cathodes for Sodium-Ion Batteries. *Adv. Energy Mater.* **2022**, *12*, 2201989. [CrossRef]
12. Gu, Z.Y.; Guo, J.Z.; Cao, J.M.; Wang, X.T.; Zhao, X.X.; Zheng, X.Y.; Li, W.H.; Sun, Z.H.; Liang, H.J.; Wu, X.L. An Advanced High-Entropy Fluorophosphate Cathode for Sodium-Ion Batteries with Increased Working Voltage and Energy Density. *Adv. Mater.* **2022**, *34*, e2110108. [CrossRef] [PubMed]
13. Jiang, J.; Li, J.; Long, X.; Zhao, D.; Su, K.; Xv, D.; Yang, C.; Qian, D. Sol–gel synthesis of $K_{1.33}Mn_8O_{16}$ nanorods and their applications for aqueous K-ion hybrid supercapacitors. *Mater. Res. Bull.* **2019**, *109*, 29–33. [CrossRef]
14. Yu, H.; Walsh, M.; Liang, X. Improving the Comprehensive Performance of $Na_{0.7}MnO_2$ for Sodium Ion Batteries by ZrO_2 Atomic Layer Deposition. *ACS Appl. Mater. Interfaces* **2021**, *13*, 54884–54893. [CrossRef] [PubMed]
15. Kaufman, J.L.; Van der Ven, A. Ordering and Structural Transformations in Layered K*x*CrO_2 for K-Ion Batteries. *Chem. Mater.* **2020**, *32*, 6392–6400. [CrossRef]
16. Lei, K.; Zhu, Z.; Yin, Z.; Yan, P.; Li, F.; Chen, J. Dual Interphase Layers in Situ Formed on a Manganese-Based Oxide Cathode Enable Stable Potassium Storage. *Chem* **2019**, *5*, 3220–3231. [CrossRef]
17. Naveen, N.; Han, S.C.; Singh, S.P.; Ahn, D.; Sohn, K.-S.; Pyo, M. Highly Stable P'3-$K_{0.8}CrO_2$ Cathode with Limited Dimensional Changes for Potassium Ion Batteries. *J. Power Sources* **2019**, *430*, 137–144. [CrossRef]
18. Sada, K.; Barpanda, P. P3-Type Layered $K_{0.48}Mn_{0.4}Co_{0.6}O_2$: A Novel Cathode Material for Potassium-Ion Batteries. *Chem. Commun.* **2020**, *56*, 2272–2275. [CrossRef]
19. Lai, Q.S.; Mu, J.J.; Liu, Z.M.; Zhao, L.K.; Gao, X.W.; Yang, D.R.; Chen, H.; Luo, W.B. Tunnel-Type $Na_2Ti_6O_{13}$@Carbon Nanowires as Anode Materials for Low-Temperature Sodium-Ion Batteries. *Batter. Supercaps* **2023**, *6*, e202200549. [CrossRef]
20. Liu, Z.; Peng, W.; Xu, Z.; Shih, K.; Wang, J.; Wang, Z.; Lv, X.; Chen, J.; Li, X. Molybdenum Disulfide-Coated Lithium Vanadium Fluorophosphate Anode: Experiments and First-Principles Calculations. *ChemSusChem* **2016**, *9*, 2122–2128. [CrossRef]
21. Liu, Z.; Wang, J.; Ding, H.; Chen, S.; Yu, X.; Lu, B. Carbon Nanoscrolls for Aluminum Battery. *ACS Nano* **2018**, *12*, 8456–8466. [CrossRef] [PubMed]
22. Liu, Z.; Wang, J.; Jia, X.; Li, W.; Zhang, Q.; Fan, L.; Ding, H.; Yang, H.; Yu, X.; Li, X.; et al. Graphene Armored with a Crystal Carbon Shell for Ultrahigh-Performance Potassium Ion Batteries and Aluminum Batteries. *ACS Nano* **2019**, *13*, 10631–10642. [CrossRef] [PubMed]

23. Shen, D.; Liu, Z.; Fan, L.; Lu, B. Organic Phosphomolybdate: A High Capacity Cathode for Potassium Ion Batteries. *Chem. Commun.* **2020**, *56*, 12753–12756. [CrossRef] [PubMed]
24. Wang, J.; Liu, Z.; Zhou, J.; Han, K.; Lu, B. Insights into Metal/Metalloid-Based Alloying Anodes for Potassium Ion Batteries. *ACS Mater. Lett.* **2021**, *3*, 1572–1598. [CrossRef]
25. Wang, J.; Zhang, G.; Liu, Z.; Li, H.; Liu, Y.; Wang, Z.; Li, X.; Shih, K.; Mai, L. $Li_3V(MoO_4)_3$ as a Novel Electrode Material with Good Lithium Storage Properties and Improved Initial Coulombic Efficiency. *Nano Energy* **2018**, *44*, 272–278. [CrossRef]
26. Yu, W.; Ge, J.; Hu, Y.; Shen, D.; Luo, W.; Chen, S.; Wu, L.; Liu, Z.; Zhou, J.; Yang, H.; et al. Hybrid High-Performance Aqueous Batteries with Potassium-Based Cathode||Zinc Metal Anode. *Sci. China Mater.* **2022**, *66*, 923–931. [CrossRef]
27. Mu, J.-J.; Liu, Z.-M.; Lai, Q.-S.; Wang, D.; Gao, X.-W.; Yang, D.-R.; Chen, H.; Luo, W.-B. An Industrial Pathway to Emerging Presodiation Strategies for Increasing the Reversible Ions in Sodium-Ion Batteries and Capacitors. *Energy Mater.* **2022**, *2*, 200043. [CrossRef]
28. Xie, C.; Liu, X.; Han, J.; Lv, L.; Zhou, X.; Han, C.; You, Y. Pomegranate-Like $KVPO_4F$@C Microspheres as High-Volumetric-Energy-Density Cathode for Potassium-Ion Batteries. *Small* **2022**, *18*, e2204348. [CrossRef]
29. Xu, J.; Duan, L.; Liao, J.; Tang, H.; Lin, J.; Zhou, X. $KVPO_4F$/Carbon Nanocomposite with Highly Accessible Active Sites and Robust Chemical Bonds for Advanced Potassium-Ion Batteries. *Green Energy Environ.* 2022; in press. [CrossRef]
30. Xu, J.; Liao, J.; Xu, Y.; Li, J.; Zhu, C.; Lin, J.; Zhou, X. Facile Synthesis of $KVPO_4F$/Reduced Graphene Oxide Hybrid as a High-Performance Cathode Material for Potassium-Ion Batteries. *J. Energy Chem.* **2022**, *68*, 284–292. [CrossRef]
31. Zhao, J.; Qin, Y.; Li, L.; Wu, H.; Jia, X.; Zhu, X.; Zhao, H.; Su, Y.; Ding, S. Pillar Strategy Enhanced Ion Transport and Structural Stability toward Ultra-Stable $KVPO_4F$ Cathode for Practical Potassium-Ion Batteries. *Sci. Bull.* **2023**, *68*, 593–602. [CrossRef] [PubMed]
32. Liao, J.; Zhang, X.; Zhang, Q.; Hu, Q.; Li, Y.; Du, Y.; Xu, J.; Gu, L.; Zhou, X. Synthesis of $KVPO_4F$/Carbon Porous Single Crystalline Nanoplates for High-Rate Potassium-Ion Batteries. *Nano Lett.* **2022**, *22*, 4933–4940. [CrossRef]
33. Liu, Z.; Wang, J.; Lu, B. Plum Pudding Model Inspired $KVPO_4F$@3DC as High-Voltage and Hyperstable Cathode for Potassium Ion Batteries. *Sci. Bull.* **2020**, *65*, 1242–1251. [CrossRef] [PubMed]
34. Tan, H.; Du, X.; Huang, J.Q.; Zhang, B. $KVPO_4F$ as a Novel Insertion-Type Anode for Potassium Ion Batteries. *Chem. Commun.* **2019**, *55*, 11311–11314. [CrossRef] [PubMed]
35. Wernert, R.; Nguyen, L.H.B.; Iadecola, A.; Weill, F.; Fauth, F.; Monconduit, L.; Carlier, D.; Croguennec, L. Self-Discharge Mechanism of High-Voltage $KVPO_4F$ for K-Ion Batteries. *ACS Appl. Energy Mater.* **2022**, *5*, 14913–14921. [CrossRef]
36. Caracciolo, L.; Madec, L.; Petit, E.; Gabaudan, V.; Carlier, D.; Croguennec, L.; Martinez, H. Electrochemical Redox Processes Involved in Carbon-Coated $KVPO_4F$ for High Voltage K-Ion Batteries Revealed by XPS Analysis. *J. Electrochem. Soc.* **2020**, *167*, 130527. [CrossRef]
37. He, X.-D.; Zhang, L.-M.; Jiang, C.-H.; Chen, C.-H. Elevating Cyclability of an Advanced $KVPO_4F$ Cathode via Multi-Component Coating Strategy for High-Performance Potassium-Ion Batteries. *Chem. Eng. J.* **2022**, *433*, 134634. [CrossRef]
38. Kim, H.; Tian, Y.; Ceder, G. Origin of Capacity Degradation of High-Voltage $KVPO_4F$ Cathode. *J. Electrochem. Soc.* **2020**, *167*, 110555. [CrossRef]
39. Liao, J.; Hu, Q.; He, X.; Mu, J.; Wang, J.; Chen, C. A Long Lifespan Potassium-Ion Full Battery Based on $KVPO_4F$ Cathode and VPO_4 Anode. *J. Power Sources* **2020**, *451*, 227739. [CrossRef]
40. Hosaka, T.; Kubota, K.; Hameed, A.S.; Komaba, S. Research Development on K-Ion Batteries. *Chem. Rev.* **2020**, *120*, 6358–6466. [CrossRef]
41. Chen, R.; Bresser, D.; Saraf, M.; Gerlach, P.; Balducci, A.; Kunz, S.; Schroder, D.; Passerini, S.; Chen, J. A Comparative Review of Electrolytes for Organic-Material-Based Energy-Storage Devices Employing Solid Electrodes and Redox Fluids. *ChemSusChem* **2020**, *13*, 2205–2219. [CrossRef] [PubMed]

Disclaimer/Publisher's Note: The statements, opinions and data contained in all publications are solely those of the individual author(s) and contributor(s) and not of MDPI and/or the editor(s). MDPI and/or the editor(s) disclaim responsibility for any injury to people or property resulting from any ideas, methods, instructions or products referred to in the content.